Persistence Diagrams of Cortical Surface Data

Moo K. Chung[1,2], Peter Bubenik[3], and Peter T. Kim[4]

[1] Department of Biostatistics and Medical Informatics
[2] Waisman Laboratory for Brain Imaging and Behavior
University of Wisconsin, Madison, WI 53706, USA
[3] Department of Mathematics
Cleveland State University, Cleveland, Ohio 44115, USA
[4] Department of Mathematics and Statistics
University of Guelph, Guelph, Ontario N1G 2W1, Canada
mkchung@wisc.edu

Abstract. We present a novel framework for characterizing signals in images using techniques from computational algebraic topology. This technique is general enough for dealing with noisy multivariate data including geometric noise. The main tool is persistent homology which can be encoded in persistence diagrams. These diagrams visually show how the number of connected components of the sublevel sets of the signal changes. The use of local critical values of a function differs from the usual statistical parametric mapping framework, which mainly uses the mean signal in quantifying imaging data. Our proposed method uses all the local critical values in characterizing the signal and by doing so offers a completely new data reduction and analysis framework for quantifying the signal. As an illustration, we apply this method to a 1D simulated signal and 2D cortical thickness data. In case of the latter, extra homological structures are evident in an control group over the autistic group.

1 Introduction

In neuroimaging, it is usually assumed that measurements f in images follow the familiar signal plus noise framework

$$f(x) = \mu(x) + \epsilon(x),\ x \in \mathbb{M} \subset \mathbb{R}^d, \tag{1}$$

where μ is the unknown mean signal, to be estimated, and ϵ is noise [3] [15] [18] [19] [25] [36]. The unknown signal is usually estimated by various spatial image smoothing over $\mathbb{M}$. The most widely used smoothing technique is kernel smoothing and its variants because of their simplicity, and because they provide the theoretical context for scale spaces and Gaussian random field theory [32] [36].

In the usual statistical parametric mapping framework [15] [19] [36], inference on the model (1) proceeds as follows. If we denote an estimate of the signal by $\widehat{\mu}$, the residual $f - \widehat{\mu}$ gives an estimate of the noise. One then constructs a test statistic $T(x)$, corresponding to a given hypothesis about the signal. As a way to account for spatial correlation of the statistic $T(x)$, the global maximum

J.L. Prince, D.L. Pham, and K.J. Myers (Eds.): IPMI 2009, LNCS 5636, pp. 386–397, 2009.

of the test statistic over the search space $\mathbb{M}$ is taken as the subsequent test statistic. Hence a great deal of the neuroimaging and statistical literature, have been devoted to determining the distribution of $\sup_{x\in\mathbb{M}} T(x)$ using random field theory [34] [36], permutation tests [30] and the Hotelling–Weyl volume of tubes calculation [29].

The use of the mean signal is one way of performing data reduction, however, this may not necessarily be the best way to characterize complex multivariate imaging data. Thus instead of using the mean signal, in this paper we propose to use what is known as persistent homology, which pairs local critical values [12] [13] [39]. It is intuitive that local critical values of $\widehat{\mu}$ approximately characterizes the shape of the continuous signal μ using only a finite number of scalar values. By pairing these local critical values in a nonlinear fashion and plotting them, one constructs the persistence diagram [7] [12] [28] [38].

Persistent homology is popular in computational algebraic topology with applications in protein structure analysis [31], gene expression [11], and sensor networks [9]. As far as the authors are aware, there is no such applications in medical image analysis even though this technique is well suited for it. This is the first paper that applies the concept of persistent homology to medical imaging data. The proposed method is illustrated using both simulated and real neuroimaging data. For the simulation, we use 1D Gaussian noise in (1) mainly for illustration. The 2D neuroimaging data comes from an MRI autism study [4] where the interest is in quantifying the abnormal cortical thickness pattern in autistic subjects if there is any. It is shown that certain persistent homology patterns unique to the autism group is evident.

2 Persistence Diagrams

A function is called a Morse function if all critical values are unique and non-degenerate, i.e. the Hessian does not vanish [27]. We note that for integer valued digital images, critical values of intensity may not be all unique; however, the underlying continuous signal μ in (1) is likely and assumed to be a Morse function. We estimate the signal using a kernel function and obtain a smooth estimate.

For illustrative purposes, we will show how to construct the persistence diagram for a 1D Morse function. Assuming μ is a Morse function with a finite number of critical values, define a sublevel set $R(y) = \mu^{-1}(-\infty, y]$. The sublevel set is the subset of $\mathbb{R}$ that satisfies $\mu(x) \leq y$. The sublevel set can have many disjoint components. Let $\#R(y)$ be the number of connected components in the sublevel set. Let us denote the local minimums as $g_1, \cdots, g_m$ and the local maximums as $h_1, \cdots, h_n$. Since the critical values of the Morse function are all unique, we can strictly order the local minimums from the smallest to the largest as

$$g_{(1)} < g_{(2)} < \cdots < g_{(m)}$$

and similarly for the local maximums as

$$h_{(1)} < h_{(2)} < \cdots < h_{(n)}.$$

We further collect all the critical values,

$$z_1 = g_1, \dots, z_m = g_m, z_{m+1} = h_1, \dots, z_{m+n} = h_n$$

and order them as

$$z_{(1)} < z_{(2)} < \cdots < z_{(m+n)}.$$

At each minimum, we have the birth of a new component, i.e.

$$\#R(g_i) = \#R(g_i - \varepsilon) + 1$$

for sufficiently small ε. The new component is identified with the local minimum g_i. Similarly at each maximum, we have the death of a component, i.e.

$$\#R(h_i) = \#R(h_i - \varepsilon) - 1,$$

and two components will merge as one. The number of connected components will only change if we pass through critical points and we can iteratively compute $\#R$ at each critical value as

$$\#R(z_{(i+1)}) = \#R(z_{(i)}) \pm 1.$$

The sign depends on whether $z_{(i+1)}$ is a maximum (-1) or a minimum $(+1)$. This is the basis of Morse theory [27] that says the topological characteristics of a topological space is characterized by the local behavior at critical points of a Morse function on that space. Persistent homology produces pairs (h_i, g_j) of critical values so that a component is born at g_j and dies at h_i. Of course these are the (topological) parameters of interest which are unknown and to be statistically estimated with data generated according to (1).

As an example, the birth and death processes are illustrated in Figure 1, where the gray dots are simulated with Gaussian noise with mean 0 and variance 0.2^2 as

$$f(x) = \mu(x) + N(0, 0.2^2)$$

with signal $\mu(t) = 10(t - 1/2)^2 + \cos(7\pi t)/2$. The signal μ is estimated using heat kernel smoothing [3] and plotted as the red line. Now we increase y from $-\infty$ to ∞. When we hit the first critical value $y = a$, the sublevel set consists of a single point, i.e. $\widehat{\#R(a)} = 1$. When we hit the minimum at $y = b$, we have the birth of a new component at b, i.e. $\widehat{\#R(b)} = 2$. When we hit the maximum at $y = c$, the two components identified by a and b are merged together to form a single component, i.e. $\widehat{\#R(c)} = 1$.

When we pass through a maximum and merge two components, we pair the maximum with the higher of the two minimums of the two components [12]. Doing so we are pairing the birth of a component to its death. Obviously the paired extremes do not have to be adjacent to each other. If there is a boundary, the function value evaluated at the boundary is treated as a critical value. In our simulated example, we need to pair (b, c) and (d, e). Other critical values are paired similarly. The reduced persistence diagram is then the scatter plot of these pairings. For technical reasons, the persistence diagram also include all of the points (a, a), where $a \in \mathbb{R}$.

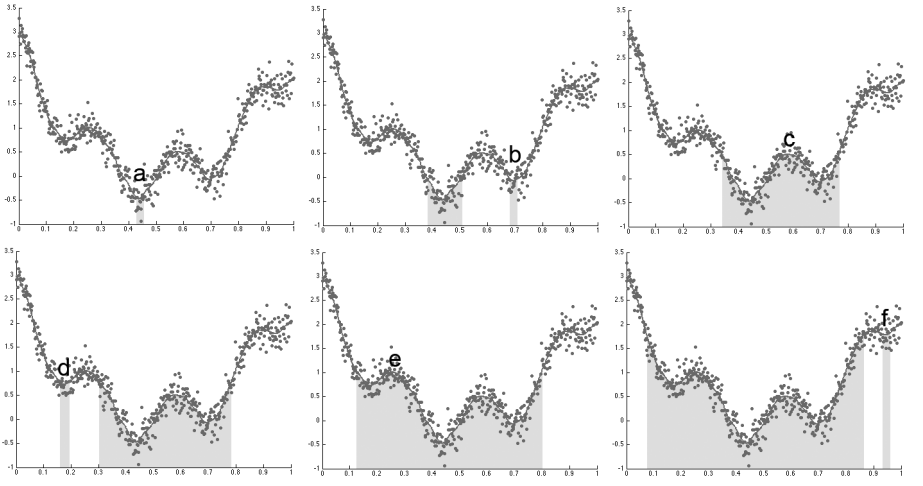

Fig. 1. The births and deaths of components in sublevel sets. We have critical values a, b, c, d, e, f, where $a < b < d < f$ are minimums and $c < e$ are maximums. At $y = a$, we have a single component marked by a single gray area. When we increase the level to $y = b$, we have the birth of a new component in addition to the existing component born at a. At the maximum $y = c$, the two components merge together to form a single component. Following the pairing rule [12], we pair (c, b) and (e, d). Other critical values are paired similarly.

2.1 Persistence Diagram for Cortical Data

For a 2D Morse function defined on a cortical manifold $\mathbb{M} \subset \mathbb{R}^3$, we need to also consider saddle points so the situation is more complicated. At a saddle point, we can have two possible pairings corresponding to either birth or death. A saddle point may join two components. This case is analogous to the local maximum in the 1D case. In this case, persistent homology pairs the value of the saddle point with the larger of the minimums of the two components. This pair is recorded as the *persistence diagram of degree* 0 (Figure 4). If the saddle point does not join two disconnected components, then a hole is born in the sublevel set. Persistent homology pairs the value at this saddle point with the value of the local maximum where this hole disappears. This pair is recorded as *the persistence diagram of degree* 1 (Figure 4). A more precise definition is given in Section 4.

Among various cortical measures, in this paper we consider cortical thickness, which has been used in characterizing various clinical populations [4] [14] [22] [23] [26] [37]. High resolution magnetic resonance images of age-matched right-handed males (16 high functioning autistic and 11 normal controls) were obtained using a 3-Tesla GE SIGNA scanner. The collected images went through intensity nonuniformity correction [33] and were spatially normalized into the MNI stereotaxic space *via* a global affine transformation [8]. Subsequently a supervised neural

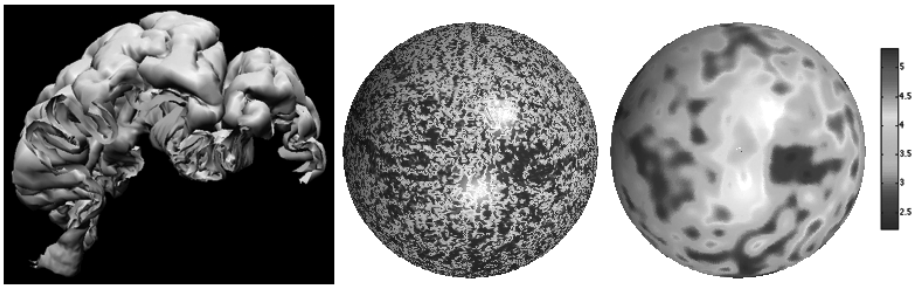

Fig. 2. Cortical thickness is computed as the distance between the outer (yellow) and the inner cortical (blue) surfaces. The cortical thickness is mapped onto a unit sphere and goes through heat kernel smoothing [3].

network classifier was used for tissue segmentation [21]. Brain substructures such as the brain stem were removed to make both the outer and the inner surfaces to be topologically equivalent to a sphere. A deformable surface algorithm [24] was used to obtain the inner cortical surface by deforming from a spherical mesh (Figure 2). Then the outer surface was obtained by deforming the inner surface. The deformation process establishes the structural correspondence between the two surfaces. The cortical thickness f is then defined as the distance between the corresponding vertices along the cortical mesh $\mathbb{M}$.

Since the deformable surface algorithm starts with a spherical mesh, there is no need to use other available surface flattening algorithms [5] [6] [16] [17] [35]

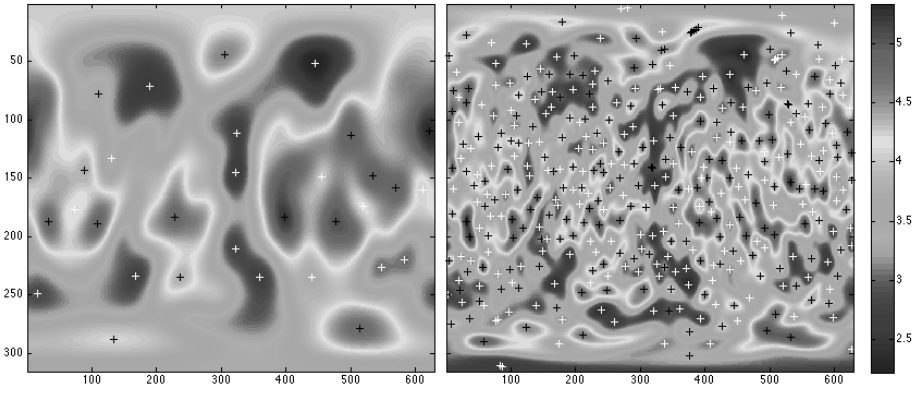

Fig. 3. The flat maps of cortical thickness at different smoothing scales. The maximums and minimums are denoted with black and white crosses respectively. The smoothing is done along the unit sphere and flattened using the angles θ (zenith angle) and φ (azimuth angle) associated with the 2-sphere. Smoother thickness produces less number of critical points and, in turn, less number of pairings.

for mapping thickness to the unit 2–sphere S^2. Let $\zeta : \mathbb{M} \to S^2$ be a sufficiently smooth surface flattening obtained from the deformable surface algorithm. Then the pullback $(\zeta^{-1})^*\widehat{\mu} = \widehat{\mu} \circ \zeta^{-1}$ projects the cortical thickness from the cortical surface $\mathbb{M}$ to the unit sphere. Figure 2 shows the pull back and the corresponding heat kernel smoothing on S^2. Note that in the process of flattening, the critical values do not change so the persistence diagram should be identical for $\widehat{\mu}$ and its pullback $(\zeta^{-1})^*\widehat{\mu}$. Therefore, we will construct the persistence diagram on the unit 2–sphere by projecting the cortical data to the sphere.

3 Kernel Smoothing

As described in Section 2.1, after the application of a deformable surface algorithm, our data is on the unit 2– sphere, S^2. So our measurement, $f : S^2 \to \mathbb{R}$ is given by the nonparametric regression formula (1), where μ is the unknown signal and ϵ is the noise. In this section, we estimate the persistent homology of the sublevel sets of $\widehat{\mu}$, an estimator of μ.

We begin by smoothing the data using the kernel,

$$K_{x_0}(x) = \max(1 - \kappa \arccos(x_0' x), 0),$$

where κ is given in [20] and $\arccos(x'y)$ gives the geodesic distance between x and y on the unit sphere. We smooth the data using the usual kernel function estimator

$$\widehat{\mu}(x) = \frac{\sum_i f(x_i) K_{x_i}(x)}{\sum_i K_{x_i}(x)}. \tag{2}$$

To implement this we need to choose the corresponding design points which we do in the following way. We start by choosing a triangulation, $\mathcal{T}$, of the sphere whose number of vertices satisfies the conditions in [1]. For our data, we start with an icosahedron and iteratively subdivide it three times, obtaining a triangulation with 1280 faces and 642 vertices.

For a sample of size n, define the estimator $\widehat{\mu}_n$ in the following way. For each vertex v in our triangulation, we define $\widehat{\mu}_n(v) = \widehat{\mu}(v)$ according to (2). For each face in our triangulation, we define $\widehat{\mu}_n$ on the face by affine interpolation from the values on the vertices. This construction is well defined on the edges, and defines a function on the sphere.

3.1 The Persistence Diagrams of $\widehat{\mu}_n$

It remains to calculate the persistence diagrams of the sublevel sets of $\widehat{\mu}_n$. We will see that because of the way $\widehat{\mu}_n$ is constructed, we can calculate its persistence diagrams using our triangulation, $\mathcal{T}$.

We filter $\mathcal{T}$ using $\widehat{\mu}_n$ as follows. Let $r_1 \leq r_2 \leq \ldots \leq r_m$ be the ordered list of values of $\widehat{\mu}_n$ on the vertices of the triangulation. For $1 \leq i \leq m$, let $\mathcal{T}_i$ be the subcomplex of $\mathcal{T}$ containing all vertices v with $\widehat{\mu}_n(v) \leq r_i$ and all edges whose

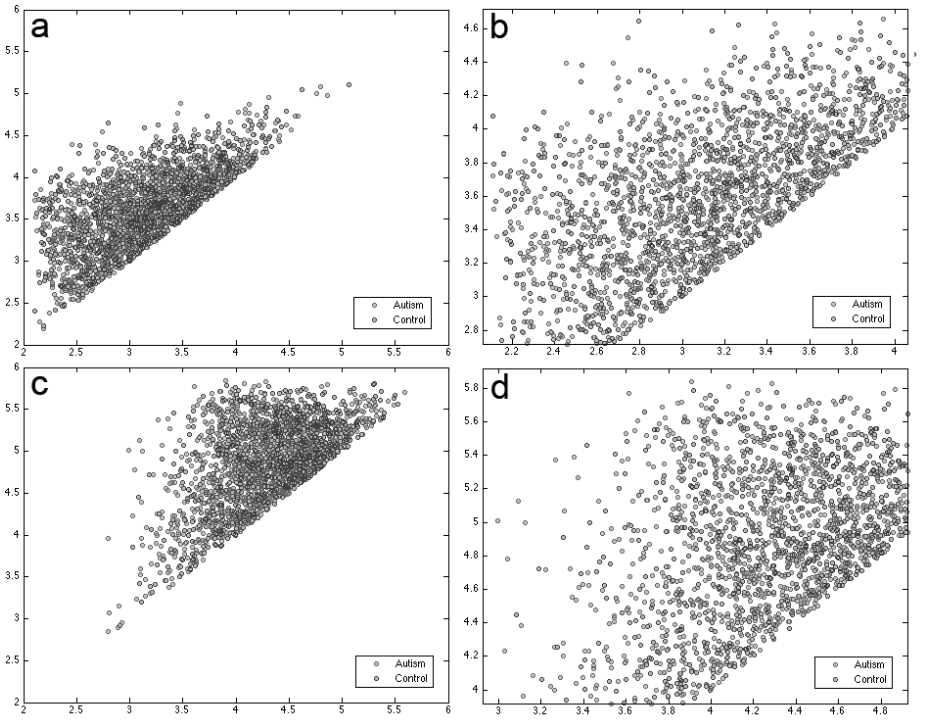

Fig. 4. The persistence diagrams for 11 control (blue) and 16 autistic (red) subjects in degree 0, (a) and (b), and degree 1, (c) and (d). One notices an additional layer of structure in the autistic group in both persistence diagrams. The figures clearly demonstrate the feasibility of using persistence diagrams for discriminating populations.

boundaries are in $\mathcal{T}_i$ and all faces whose boundaries are in $\mathcal{T}_i$. We obtain the following filtration of $\mathcal{T}$,

$$\phi = \mathcal{T}_0 \subset \mathcal{T}_1 \subset T_2 \subset \cdots \subset \mathcal{T}_m = \mathcal{T}.$$

The end result is that the topological properties of the sublevel sets of $\widehat{\mu}_n$ will equal the topological properties of the above filtration of $\mathcal{T}$.

Using the software Plex, [10], we calculate the persistent homology, in degrees 0, 1 and 2 of the triangulation $\mathcal{T}$ filtered according to the estimator for each of the 27 subjects. Since the data is two–dimensional, we do not expect any interesting homology in higher degrees. In degree two, the persistent homology consists of a single persistence pair (a, ∞), where a is the maximum of $\widehat{\mu}_n$.

To compare the autistic subjects and control subjects, we take the union of the persistence diagrams of the subjects (Figure 4).

4 Statistical Properties of Persistence Diagram

In this section we will make more precise the definition of a persistence diagram [7] and present results that compare the topological parameters and their estimators [1] [2].

The persistent homology of the signal, μ, is encoded in its reduced persistence diagram, $\bar{D}(\mu)$, which is a multiset of points each corresponding to the persistence of one topological feature, as in the examples above. In order to define a metric for such diagrams, it is convenient to add the ordered pairs (a, a) for all $a \in \mathbb{R}$, each with infinite multiplicity. Call this multiset the *persistence diagram* of μ, denoted $D(\mu)$. We now give the precise definition.

Let k be a nonnegative integer. Given $\mu : S^2 \to \mathbb{R}$ and $a \leq b \in \mathbb{R}$ the inclusion of sublevel sets $i_a^b : S^2_{\mu \leq a} \hookrightarrow S^2_{\mu \leq b}$ induces a map on homology

$$H_k(i_a^b) : H_k(S^2_{f \leq a}) \to H_k(S^2_{f \leq b}).$$

The image of $H_k(i_a^b)$ is the persistent homology group from a to b and $S^2_{f \leq c} = \{f(x) \leq c\}$. Let β_a^b be its dimension. This counts the independent homology classes which are born by time a and die after time b.

Call a real number a a *homological critical value* of μ if for all sufficiently small $\varepsilon > 0$ the map $H_k(i_{a-\varepsilon}^{a+\varepsilon})$ is not an isomorphism. Call μ *tame* if it has finitely many homological critical values, and for each $a \in \mathbb{R}$, $H_k(S^2_{\mu \leq a})$ is finite dimensional. In particular, any Morse function on a compact manifold is tame.

Assume that μ is tame. Choose ε smaller than the distance between any two homological critical values. For each pair of homological critical values $a < b$, we define their *multiplicity* μ_a^b which we interpret as the number of independent homology classes that are born at a and die at b. We count the homology classes born by time $a + \varepsilon$ that die after time $b - \varepsilon$. Among these subtract those born by $a - \varepsilon$ and subtract those that die after $b + \varepsilon$. This double counts those born by $a - \varepsilon$ that die after $b + \varepsilon$, so we add them back. That is,

$$\mu_a^b = \beta_{a+\varepsilon}^{b-\varepsilon} - \beta_{a-\varepsilon}^{b-\varepsilon} - \beta_{a+\varepsilon}^{b+\varepsilon} + \beta_{a-\varepsilon}^{b+\varepsilon}.$$

The *reduced persistence diagram* of μ, $\bar{D}(\mu)$, is the multiset of pairs (b, a) together with their multiplicities μ_a^b. We call this a diagram since it is convenient to plot these points on the plane. We will see that it is useful to add homology classes which are born and die at the same time. Let the *persistence diagram* of μ, $D(\mu)$, be given by the union of $\bar{D}(\mu)$ and $\{(a, a)\}_{a \in \mathbb{R}}$ where each (a, a) has infinite multiplicity.

A metric on the space of persistence diagrams is the bottleneck distance which bounds the Hausdorff distance [7]. It is given by

$$d_B(D(\mu), D(\nu)) = \inf_{\gamma} \sup_{p \in D(\mu)} \|p - \gamma(p)\|_\infty, \tag{3}$$

where the infimum is taken over all bijections $\gamma : D(\mu) \to D(\nu)$ and $\|\cdot\|_\infty$ is the sup-norm metric. In [7], the following result is proven:

$$d_B(D(\mu), D(\nu)) \leq \|\mu - \nu\|_\infty \tag{4}$$

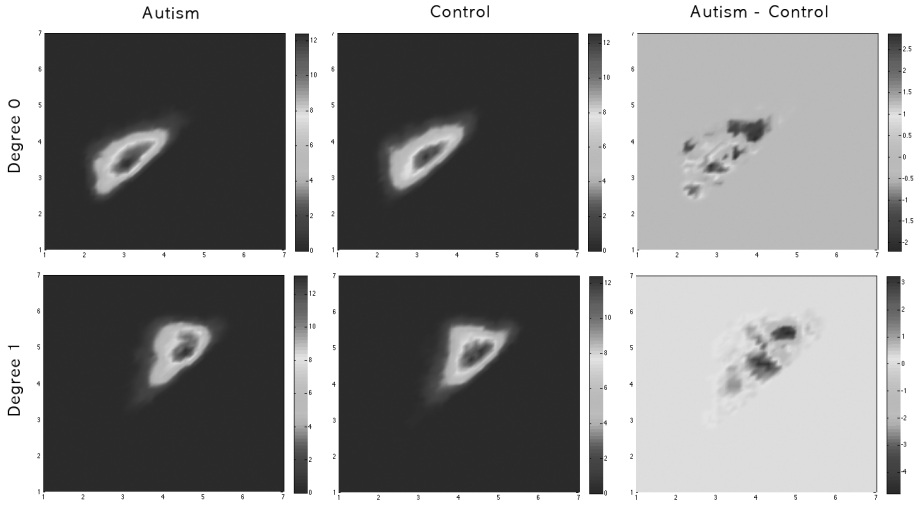

Fig. 5. The pairing concentration is computed by counting the number of pairings within a circle of fixed radius 0.2 at the point $x \in [1,7]^2$. The first (second) row is the mean concentration map for degree 0 (1) persistence. The first (second) column is the concentration map of autistic (control). The concentration difference (autism - control) is given in the last column which shows concentration difference between the groups.

where $\mu, \nu : \mathbb{M} \to \mathbb{R}$ are tame functions. As an immediate consequence of (4), we can apply it to the model (1). Let $\Lambda_t(\beta, L)$ denote the subset of tame functions in $\Lambda(\beta, L)$ the class of Hölder functions

$$\Lambda(\beta, L) = \{f : S^2 \to \mathbb{R} \mid |f(x) - f(z)| \leq L(\arccos(x'y))^\beta, x, z \in S^2\}, \quad (5)$$

where $0 < \beta \leq 1$ and $L > 0$.

If we assume $\mu \in \Lambda_t(\beta, L)$ for the model (1) ϵ is $N(0, \sigma^2)$, for the estimator $\widehat{\mu}_n$ with $0 < \beta \leq 1$ and $L > 0$,

$$\sup_{\mu \in \Lambda_t(\beta,L)} \mathbb{E} d_B \left(D(\hat{\mu}_n), D(\mu)\right) \leq L^{2/(2\beta+2)} \left(\frac{\sigma^2 \ (\beta+2)2^3}{\beta^2} \ \frac{\log n}{n}\right)^{\beta/(2\beta+2)} \quad (6)$$

as $n \to \infty$ [1], where expectation $\mathbb{E}$ is with respect to the model (1).

For typical brain images ($L = \beta = \sigma^2 = 1$) using (6), the order of accuracy per individual is $10^{-3/2}$. Consequently, Figure 4 is an accurate description of the population parameters.

5 Discussion

We have presented the concept of persistence diagrams and described the filtration based algorithm for constructing them. Since cortical thickness is highly

noisy, kernel smoothing is applied to remove high frequency spatial noise before the filtration. At this point, it is unclear how one determines the possible statistical significance of persistent diagram difference. One may be tempted to use hypothesis-free classification frameworks for inference, however, Figure 4 shows that classification based on possibly discriminating spatial pattern is likely to be challenging. Note that the autistic scatter plots basically encompass the control scatter plots for the degree 0 and degree 1 persistence diagrams. Since there is considerable overlap, machine learning techniques would need to be adapted for this challenge. On the other hand, there seems to be spatial concentration difference in the pairings.

We have computed the pairing concentration by computing the number of parings within a circle of radius 0.2 at the point $x \in [1, 7]^2$. The average pairing concentration maps are shown in Figure 5, where we can see concentration difference for both the degree 0 and 1 persistence diagrams. The significance of the concentration map difference is determined using a permutation test. We first constructed the two sample t statistic map $T(p)$. The type-I error for correcting for multiple comparisons of a one-sided test is given by $\sup_{p\in[1,7]^2} T(p)$ [36]. The empirical distribution of $\sup_{p\in[1,7]^2} T(p)$ is then estimated from 5000 random permutations. For the degree-0 persistence, we obtain the maximum T-stat value of 3.51 corresponding to the corrected p-value of 0.078 at the position (2.3, 4.2). For the degree-1 persistence, the maximum T-stat value is 3.95 corresponding to the corrected p-value of 0.021 at the position (5.5, 5.8).

Our finding is consistent with previous neuroanatomical studies that show the abnormal neuroanatomical structures for autistic subjects [4]. Here we only presented a simple nonparametric approach for determining statistical significance based on the pairing concentration. Possibly a better statistical inference procedure is needed. It is hoped that this paper presents itself as a spring board for further investigation of persistence diagram based characterization of medical images. There are many methodological issues we have not discussed such as rigorous inferential procedures or the estimation of confidence regions around paired points possibly *via* the bootstrap. These are the next challenges in future works.

Acknowledgment

Authors wish to thank Vikas Singh of the University of Wisconsin-Madison for discussion on the persistence diagram. PK's research was supported in part by NSERC (Canada). Kim M. Dalton and Richard J. Davidson of the Waisman Laboratory for Brain Imaging and Behavior provided the MRI data used in the study.

References

1. Bubenik, P., Carlsson, G., Kim, P.T., Luo, Z.: Asymptotic minimax sup-norm risk on manifolds with application to topology (preprint, 2008)
2. Bubenik, P., Kim, P.T.: A statistical approach to persistent homology. Homology, Homotopy and Applications 9, 337–362 (2007)

3. Chung, M.K., Shen, L., Dalton, K.M., Evans, A.C., Davidson, R.J.: Weighted fourier representation and its application to quantifying the amount of gray matter. IEEE Transactions on Medical Imaging 26, 566–581 (2007)
4. Chung, M.K., Robbins, S., Davidson, R.J., Alexander, A.L., Dalton, K.M., Evans, A.C.: Cortical thickness analysis in autism with heat kernel smoothing. NeuroImage 25, 1256–1265 (2005)
5. Angenent, S., Hacker, S., Tannenbaum, A., Kikinis, R.: On the laplace-beltrami operator and brain surface flattening. IEEE Transactions on Medical Imaging 18, 700–711 (1999)
6. Brechbuhler, C., Gerig, G., Kubler, O.: Parametrization of closed surfaces for 3D shape description. Computer Vision and Image Understanding 61, 154–170 (1995)
7. Cohen-Steiner, D., Edelsbrunner, H., Harer, J.: Stability of persistence diagrams. Discrete and Computational Geometry 37 (2007)
8. Collins, D.L., Neelin, P., Peters, T.M., Evans, A.C.: Automatic 3d intersubject registration of MR volumetric data in standardized talairach space. J. Comput. Assisted Tomogr. 18, 192–205 (1994)
9. Ghrist, R., de Silva, V.: Homological sensor networks. Notic. Amer. Math. Soc. 54, 10–17 (2007)
10. de Silva, V., Perry, P.: Plex version 2.5 (2005), `http://math.stanford.edu/comptop/programs/plex`
11. Dequent, M.-L., Mileyko, Y., Edelsbrunner, H., Pourquie, O.: Assessing periodicity in gene expression as measured by microarray data (preprint, 2008)
12. Edelsbrunner, H., Harer, J.: Persistent homology - a survey. In: Twenty Years After, American Mathematical Society (2008) (in press)
13. Edelsbrunner, H., Letscher, D., Zomorodian, A.: Topological persistence and simplification. Discrete and Computational Geometry 28, 511–533 (2002)
14. Fischl, B., Dale, A.M.: Measuring the thickness of the human cerebral cortex from magnetic resonance images. PNAS 97, 11050–11055 (2000)
15. Friston, K.J.: A short history of statistical parametric mapping in functional neuroimaging. Technical Report Technical report, Wellcome Department of Imaging Neuroscience, ION, UCL., London, UK (2002)
16. Gu, X., Wang, Y.L., Chan, T.F., Thompson, T.M., Yau, S.T.: Genus zero surface conformal mapping and its application to brain surface mapping. IEEE Transactions on Medical Imaging 23, 1–10 (2004)
17. Hurdal, M.K., Stephenson, K.: Cortical cartography using the discrete conformal approach of circle packings. NeuroImage 23, S119–S128 (2004)
18. Joshi, S.C.: Large Deformation Diffeomorphisms and Gaussian Random Fields For Statistical Characterization of Brain Sub-manifolds. Ph.D. thesis. Washington University, St. Louis (1988)
19. Kiebel, S.J., Poline, J.-P., Friston, K.J., Holmes, A.P., Worsley, K.J.: Robust smoothness estimation in statistical parametric maps using standardized residuals from the general linear model. NeuroImage 10, 756–766 (1999)
20. Klemelä, J.: Asymptotic minimax risk for the white noise model on the sphere. Scand. J. Statist. 26, 465–473 (1999)
21. Kollakian, K.: Performance analysis of automatic techniques for tissue classification in magnetic resonance images of the human brain. Technical Report Master's thesis, Concordia University, Montreal, Quebec, Canada (1996)
22. Lerch, J.P., Evans, A.C.: Cortical thickness analysis examined through power analysis and a population simulation. NeuroImage 24, 163–173 (2005)

23. Luders, E., Narr, K.L., Thompson, P.M., Rex, D.E., Woods, R.P., Jancke, L., Toga, A.W., DeLuca, H.: Gender effects on cortical thickness and the influence of scaling. Human Brain Mapping 27, 314–324 (2006)
24. MacDonald, J.D., Kabani, N., Avis, D., Evans, A.C.: Automated 3-D extraction of inner and outer surfaces of cerebral cortex from MRI. NeuroImage 12, 340–356 (2000)
25. Miller, M.I., Banerjee, A., Christensen, G.E., Joshi, S.C., Khaneja, N., Grenander, U., Matejic, L.: Statistical methods in computational anatomy. Statistical Methods in Medical Research 6, 267–299 (1997)
26. Miller, M.I., Massie, A.B., Ratnanather, J.T., Botteron, K.N., Csernansky, J.G.: Bayesian construction of geometrically based cortical thickness metrics. NeuroImage 12, 676–687 (2000)
27. Milnor, J.: Morse Theory. Princeton University Press, Princeton (1973)
28. Morozov, D.: Homological Illusions of Persistence and Stability. Ph.D. thesis, Duke University (2008)
29. Naiman, D.Q.: Volumes for tubular neighborhoods of spherical polyhedra and statistical inference. Ann. Statist. 18, 685–716 (1990)
30. Nichols, T., Hayasaka, S.: Controlling the familywise error rate in functional neuroimaging: a comparative review. Stat. Methods Med. Res. 12, 419–446 (2003)
31. Ozturk, O., Ferhatosmanoglu, H., Sacan, A., Wang, Y.:
32. Siegmund, D.O., Worsley, K.J.: Testing for a signal with unknown location and scale in a stationary gaussian random field. Annals of Statistics 23, 608–639 (1996)
33. Sled, J.G., Zijdenbos, A.P., Evans, A.C.: A nonparametric method for automatic correction of intensity nonuniformity in MRI data. IEEE Transactions on Medical Imaging 17, 87–97 (1988)
34. Taylor, J.E., Worsley, K.J.: Random fields of multivariate test statistics, with applications to shape analysis. Annals of Statistics 36, 1–27 (2008)
35. Timsari, B., Leahy, R.: An optimization method for creating semi-isometric flat maps of the cerebral cortex. In: The Proceedings of SPIE, Medical Imaging (2000)
36. Worsley, K.J., Marrett, S., Neelin, P., Vandal, A.C., Friston, K.J., Evans, A.C.: A unified statistical approach for determining significant signals in images of cerebral activation. Human Brain Mapping 4, 58–73 (1996)
37. Yezzi, A., Prince, J.L.: An eulerian pde approach for computing tissue thickness. IEEE Transactions on Medical Imaging 22, 1332–1339 (2003)
38. Zomorodian, A.J.: Computing and Comprehending Topology: Persistence and Hierarchical Morse Complexes. Ph.D. Thesis, University of Illinois, Urbana-Champaign (2001)
39. Zomorodian, A.J., Carlsson, G.: Computing persistent homology. Discrete and Computational Geometry 33, 249–274 (2005)